

1 **The Influence of Assimilating Leaf Area Index in a Land Surface**
2 **Model on Global Water Fluxes and Storages**

3

4 Xinxuan Zhang¹, Viviana Maggioni¹, Azbina Rahman¹, Paul Houser¹, Yuan Xue¹, Timothy
5 Sauer¹, Sujay Kumar² and David Mocko²

6

7 1. George Mason University, Fairfax, VA, USA

8 2. Hydrological Sciences Laboratory, NASA Goddard Space Flight Center, Greenbelt, MD, USA

9

10

11

12

13

14

15

16

17

18

Submit to:

19

Hydrology and Earth System Sciences

20

March, 2020

21

22

Abstract

23
24 Vegetation plays a fundamental role not only in the energy and carbon cycles, but also in the global
25 water balance by controlling surface evapotranspiration (ET). Thus, accurately estimating
26 vegetation-related variables has the potential to improve our understanding and estimation of the
27 dynamic interactions between the water, energy, and carbon cycle. This study aims to assess to
28 what extent a land surface model (LSM) can be optimized through the assimilation of leaf area
29 index (LAI) observations at the global scale. Two Observing System Simulation Experiments
30 (OSSEs) are performed to evaluate the efficiency of assimilating LAI into an LSM through an
31 Ensemble Kalman Filter (EnKF) to estimate LAI, ET, canopy interception evaporation (CIE),
32 canopy water storage (CWS), surface soil moisture (SSM), and terrestrial water storage (TWS).
33 Results show that the LAI data assimilation framework not only effectively reduces errors in LAI
34 model simulations, but also improves all the modeled water flux and storage variables considered
35 in this study (ET, CIE, CWS, SSM, and TWS), even when the forcing precipitation is strongly
36 positively biased (extremely wet condition). However, it tends to worsen some of the modeled
37 water-related variables (SSM and TWS) when the forcing precipitation is affected by a dry bias.
38 This is attributed to the fact that the amount of water in the LSM is conservative and the LAI
39 assimilation introduces more vegetation, which requires more water than what available within the
40 soil.
41

42 **1. Introduction**

43 Terrestrial vegetation plays a vital role in the global water cycle, as it controls the surface
44 evapotranspiration (ET) and the state of the carbon cycle. As shown in past literature, there exists
45 a strong relationship among vegetation, precipitation, and soil moisture (Di et al., 1994; Farrar et
46 al., 1994; Richard and Pocard, 1998; Adegoke and Carleton, 2002). Nevertheless, the role that
47 vegetation and its dynamics play in the water cycle (for instance on the variability of precipitation)
48 is extremely complex (Wang and Eltahir 2000; Wang et al. 2011). In the past half-century, these
49 land surface processes and feedbacks have been examined through numerical modeling
50 experiments (Foley et al. 1996; Kim and Wang 2007; Druel et al. 2019). In early generation land
51 surface models (LSMs), the development stage of vegetation was prescribed by regularly updating
52 vegetation variables, based on fixed lookup tables to simplify the model computation (Foley et al.
53 1996). This approach uses constant vegetation indices, e.g., the leaf area index (LAI), while in
54 reality the growth of vegetation continuously changes in response to weather and climate
55 conditions. To overcome this deficiency, new generation LSMs are coupled with dynamic
56 vegetation modules that comprehensively simulate several biogeochemical processes (Woodward
57 and Lomas 2004; Gibelin et al. 2006; Fisher et al. 2018) and that are able to capture more detailed
58 variations in plant productivity than traditional methods (Kucharik et al. 2000; Arora 2002;
59 Krinner et al. 2005).

60 LAI can also be estimated through observations from satellite sensors, such as the
61 Moderate Resolution Imaging Spectroradiometer (MODIS, Pagano and Durham 1993; Justice et
62 al. 2002), the Système Probatoire d'Observation de la Terre VEGETATION (SPOT-VGT, Baret
63 et al. 2007), and the National Oceanic and Atmospheric Administration (NOAA) Advanced Very
64 High Resolution Radiometer (AVHRR, Cracknell 1997). LAI products retrieved from different

65 satellite missions and sensors provide spatially and temporally varying LAI fields on a routine
66 basis at regional and global scales, including the MODIS LAI (Myneni et al. 2002), the Global
67 Land Surface Satellite (GLASS) LAI (Xiao et al. 2013), and the GLOBMAP LAI dataset (Liu et
68 al. 2012), among others. Satellite-derived LAI products were found to be affected by uncertainties
69 due to the limitation of retrieval algorithms and vegetation type sampling issues (Cohen and Justice
70 1999; Privette et al. 2002; Tian et al. 2002; Morisette et al. 2002).

71 A method to combine the inherently incorrect estimates from satellite observations and
72 model simulations is data assimilation (DA). One of the most common DA systems — the
73 Ensemble Kalman Filter (EnKF; Evensen 2003) — dynamically updates the model error
74 covariance information by producing an ensemble of model predictions, which are individual
75 model realizations perturbed by the assumed model error (Reichle et al. 2007). The ensemble
76 approach is widely used in hydrology because of its flexibility with respect to the type of model
77 error (Crow and Wood 2003) and well suited to the nonlinear nature of land surface processes
78 (Reichle et al. 2002a, 2002b; Andreadis and Lettenmaier 2006; Durand and Margulis 2008; Kumar
79 et al. 2008; Pan and Wood 2006; Pauwels and De Lannoy 2006; Zhou et al. 2006). However, the
80 use of an EnKF for the assimilation of LAI in LSMs has not been thoroughly investigated in the
81 past. Pauwels et al. (2007) proposed an Observing System Simulation Experiment (OSSE) to
82 evaluate the performance of assimilating LAI in a hydrology-crop growth model with an EnKF
83 algorithm. Other studies have also tested simplified 1D-VAR and extended Kalman filter methods
84 for LAI assimilation (e.g., Sabater et al. 2008; Barbu et al. 2011; Fairbairn et al. 2017). Recently,
85 Kumar et al. (2019) assimilated GLASS LAI in a land surface model with an EnKF across the
86 continental U.S. Some water budget variables were improved through the assimilation procedure,
87 particularly in agricultural areas where the assimilation added harvesting information to the model.

88 Ling et al. (2019) assimilated global LAI information with an Ensemble Adjust Kalman Filter
89 (EAKF) algorithm and found that the assimilation is more effective during the growing season.
90 LAI assimilation also had a positive impact on gross primary production (GPP) and ET in low
91 latitude regions.

92 Nevertheless, most of the aforementioned studies mainly focused on the impact of LAI
93 assimilation on the simulated LAI or vegetation biomass. Only a few studies discussed the
94 influences of LAI assimilation on the estimation of water variables such as soil moisture or
95 streamflow (Pauwels et al. 2007; Sabater et al. 2008) and most of them focused on limited regions.
96 Most recently, Albergel et al. (2017) conducted a study on a much larger domain – Europe and the
97 Mediterranean basin –and showed improvement in soil moisture at various depths thanks to LAI
98 assimilation.

99 This work leverages upon these studies but aims to assess to what extent a land surface
100 model, especially the simulation of water-related variables, can be optimized through the
101 assimilation of LAI observations at the global scale. As this study serves as a feasibility test to
102 quantify the impact of LAI assimilation on water cycle variables, an OSSE is chosen to investigate
103 the model’s behavior. This guarantees that reference variables (often referred to as the “truth”),
104 which are synthetically produced, are available for quantifying the performance of the proposed
105 framework. Specifically, two OSSEs that apply an EnKF algorithm to the Noah LSM with multi-
106 parameterization options (Noah-MP, Niu et al. 2011; Yang et al. 2011) are performed to evaluate
107 the efficiency of assimilating LAI observations for estimating ET, canopy interception evaporation
108 (CIE), canopy water storage (CWS), surface soil moisture (SSM), and terrestrial water storage
109 (TWS).

110

111

112 **2. Methods and materials**

113 *2.1. Land surface model (Noah-MP)*

114 The Noah-MP 3.6 (Niu et al. 2011; Yang et al. 2011) is adopted in this study. Noah-MP contains
115 a separate vegetation canopy defined by a canopy top and bottom, crown radius, and leaves with
116 defined dimensions, orientation, density, and radiometric properties (Niu et al. 2011). Multiple
117 options are available for surface water infiltration, runoff, groundwater transfer and storage
118 including water table depth to an unconfined aquifer (Niu et al. 2007), dynamic vegetation, canopy
119 resistance, and frozen soil physics. Specifically, the prognostic vegetation growth combines a Ball-
120 Berry photosynthesis-based stomatal resistance (Ball et al. 1987) with a dynamic vegetation model
121 (Dickinson et al. 1998). The dynamic vegetation model calculates the carbon storages in various
122 parts of the vegetation (leaf, stem, wood, and root) and the soil carbon pools.

123 The Noah-MP 3.6 LSM has been implemented into the National Aeronautics and Space
124 Administration (NASA) Land Information System (LIS; Peters-Lidard et al. 2007; Kumar et al.
125 2006). LIS is a software that provides an interagency test bed for land surface modeling and data
126 assimilation that allows customized systems to be built, assembled and reconfigured easily, using
127 shared plugins and standard interfaces. All the experiments in this study are setup through LIS.
128 The Modern-Era Retrospective analysis for Research and Applications Version 2 (MERRA-2;
129 Gelaro et al. 2017) dataset serves as the meteorological forcings of Noah-MP. MERRA-2 is the
130 latest atmospheric reanalysis produced by the NASA Global Modeling and Assimilation Office
131 (GMAO) and includes updates from the Goddard Earth Observing System (GEOS). The
132 meteorological variables selected from MERRA-2 include surface pressure, surface air
133 temperature, surface specific humidity, incident radiations, wind speed, and precipitation rate.

134 Five model output variables that describe terrestrial water fluxes and storages are
135 investigated in this work: ET (defined as the sum of evaporation and the plant transpiration
136 [kg/m²s]), CIE (defined as the evaporation of the canopy intercepted water [kg/m²s]), CWS
137 (defined as the amount of canopy intercepted water in both liquid and ice phases [kg/m²]), SSM
138 (defined as the water content in the top 10 cm of the soil column [m³/m³]), and TWS (defined as
139 the sum of all water storage on the land surface and in the subsurface [mm]).

140

141 *2.2. Experimental design*

142 An OSSE is designed to understand the efficiency of assimilating LAI within Noah-MP version
143 3.6 using a one-dimensional EnKF algorithm (Reichle et al. 2010), when the precipitation forcing
144 data are strongly biased. Being the major driving force of the hydrological cycle, the quality of
145 input precipitation is critical for the accuracy of land surface model outputs. However, global
146 precipitation datasets are far from being perfect and often affected by large regional biases. For
147 example, the MERRA-2 precipitation dataset shows a widespread relative bias greater than 100%
148 in South Asia (Ghatak et al. 2018). Although an EnKF is optimal only under the assumption of
149 unbiasedness (which is not met in the proposed experimental setup), we want to investigate here
150 to what extent the EnKF LAI assimilation (even if sub-optimal) can improve water storages and
151 fluxes under two extreme conditions, i.e., a very dry and a very wet precipitation bias, knowing
152 that such biases are very plausible in the real world and often unknown (and therefore difficult to
153 remove). The proposed framework is evaluated through a global experiment (Antarctica excluded)
154 at the $0.625^\circ \times 0.5^\circ$ spatial resolution of the MERRA-2 forcing dataset (Figure 1).

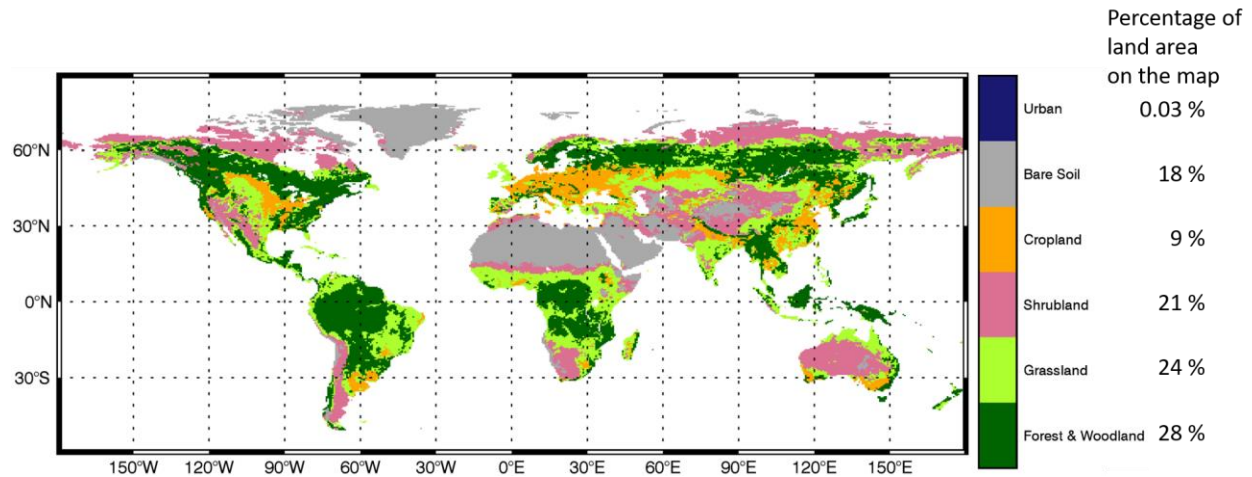


Figure 1. Study domain and land cover types (Hansen et al. 2000).

155

156

157

158

159

160

161

162

163

164

165

166

167

168

169

170

171

Figure 2 shows a schematic diagram of the experiments. First, the Noah-MP model is spun-up for a 10-year period (2001-2010) to ensure a physically realistic state of equilibrium. Second, the model is run for a 29-month period (January 2011 – May 2013) to conduct the Nature Run (NR) with the same configuration as the spin-up one. By definition, an OSSE is a controlled experiment that does not assimilate any real observation. Instead, it treats all the model outputs from the NR as the “true” condition (denoted as the “synthetic truth”). The “true” LAI (i.e., the LAI output from NR) is then perturbed via a simple additive error model to produce the synthetic observations to be assimilated into the DA runs. The spin-up run and NR are forced by the original MERRA-2 precipitation data. Third, two Open Loop (OL) runs (no DA) are conducted for the same 29-month period under two conditions: i) “extremely dry” condition (the model is forced by halving the MERRA-2 precipitation data; OL-dry), and ii) “extremely wet” condition (the model is forced by doubling the MERRA-2 precipitation; OL-wet). The biased forcing precipitation data in OL mimic typical precipitation biases in current precipitation reanalysis and satellite products (e.g., Ghatak et al. 2018; Yoon et al. 2019).

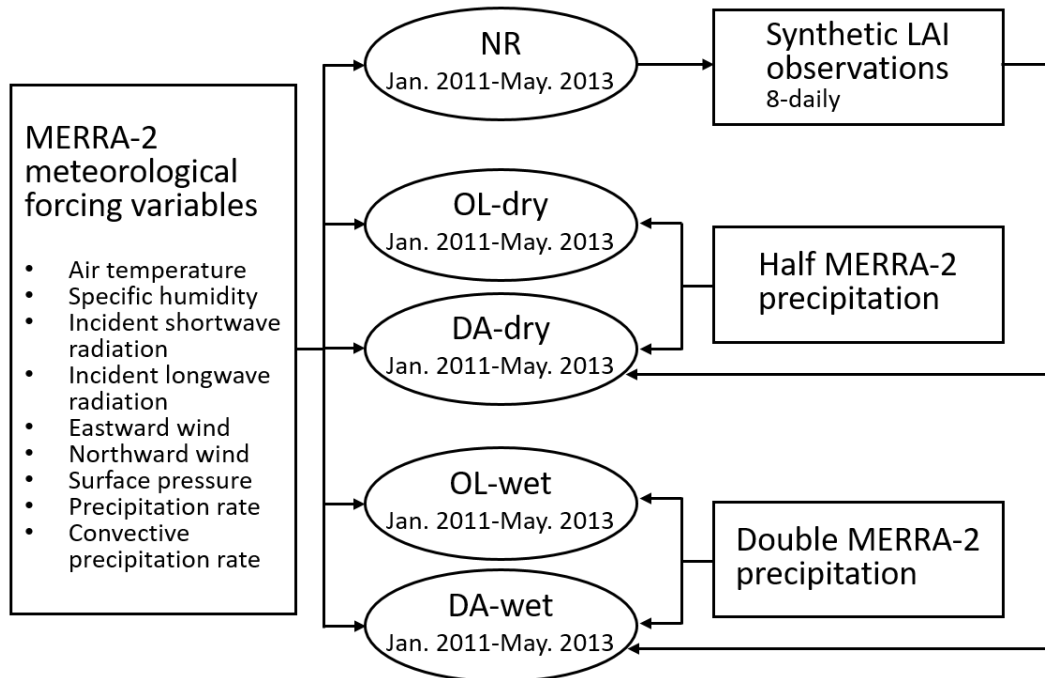


Figure 2. Schematic diagram of the OSSE design.

172

173

174

175 The two DA runs are then conducted under the two same conditions (DA-dry and DA-wet)
 176 using a one-dimensional EnKF assimilation algorithm, which is a built-in DA method in LIS. The
 177 EnKF DA algorithm is suitable for non-linear and intermittent land surface processes (Reichle et
 178 al. 2002a, 2002b). Details of the algorithm can be found in numerous previous studies (Reichle et
 179 al. 2010; De Lannoy et al. 2012; Liu et al. 2015; Kumar et al. 2019a).

180 The model ensemble is generated by perturbing a set of meteorological forcing. To select
 181 the optimal ensemble size, a sensitivity test is performed for ensemble sizes spanning from 2 to 24
 182 members (not shown here). The number of ensemble members has a strong impact on the model
 183 results at small sizes, while the model performance tends to become steady when more than 20
 184 ensemble members are considered. Thus, all the DA simulations are run for 20 members.

185 The synthetic LAI observations are obtained from the NR and assimilated to the DA system
 186 at 8-daily frequency. The synthetic LAI observation has the same temporal resolution as the

187 MODIS LAI product but with full coverage over the study domain. In real case studies, satellite
188 LAI products contain a substantial amount of missing data, mainly due to the cloud obscuration
189 gaps. Based on the vegetation type in the model, the leaf mass fields are also updated. Random
190 perturbations of MERRA-2 meteorological forcings and synthetic LAI observations are applied to
191 create an ensemble of land surface conditions that represent the uncertainties of in the LSM.

192 Similar to previous work (Kumar et al. 2014, 2019a, 2019b), the MERRA-2 forcing inputs
193 such as shortwave/longwave radiations and precipitation are perturbed hourly. Multiplicative
194 perturbations are applied to the shortwave radiation and precipitation with a mean of 1 and standard
195 deviations of 0.3 and 0.5, respectively. The longwave radiation is perturbed via an additive
196 perturbation with a standard deviation of 50 W/m². The perturbations of the three meteorological
197 forcing variables also include cross correlations: cross correlation between shortwave radiation
198 and precipitation is -0.8, cross correlation between longwave radiation and precipitation is 0.5; and
199 cross correlation between shortwave and longwave radiations is -0.5. The synthetic LAI
200 observations are perturbed via an additive model with a standard deviation of 0.1.

201

202 ***2.3. Evaluation and error metrics***

203 Output variables from the OL and DA runs are evaluated against the “truth” from the NR at daily,
204 monthly, and seasonal temporal scales. Besides LAI, five more water fluxes and storages are
205 evaluated in the results section: ET, CIE, CWS, SSM, and TWS.

206 The initial condition for the OL and DA runs is generated by a spin-up run that uses the
207 original MERRA-2 precipitation as input. However, the OL and DA runs are forced by either
208 doubled or halved precipitation, which is not consistent with the spin-up run and the model needs
209 some time to stabilize. The first 5-month model outputs are therefore eliminated from the

210 evaluation to avoid the model systematic instability at the beginning of the OL and DA simulations
 211 and the evaluation, thus, focused only on model outputs from 2011-06-01 to 2013-05-31. Results
 212 are discussed using maps and time series of global averaged values and anomalies. Each of the
 213 anomaly time series is computed relative to the mean of its respective model run. Moreover, two
 214 error metrics are employed to quantify the difference between OL (and DA) with respect to the
 215 reference variables (from the NR). The first one is the Normalized and Centered Root Mean Square
 216 Error (NCRMSE), defined as follows:

$$217 \quad E = \frac{\left\{ \frac{1}{N} \sum_{i=1}^N [(X_i - \text{mean}(X)) - (O_i - \text{mean}(O))]^2 \right\}^{\frac{1}{2}}}{\text{mean}(O)} \quad \text{Eq. 1}$$

218 where E is the NCRMSE, O is the NR output variable, and X is the output variable from the OL
 219 runs or DA runs. N is the total number of X values, and i represents the index of each X value.
 220 Second, to investigate the improvement (or degradation) due to the DA of LAI observations, we
 221 adopt the Normalized Information Contribution (NIC, similar to the NIC in Kumar et al. 2016)
 222 index based on NCRMSE and defined as:

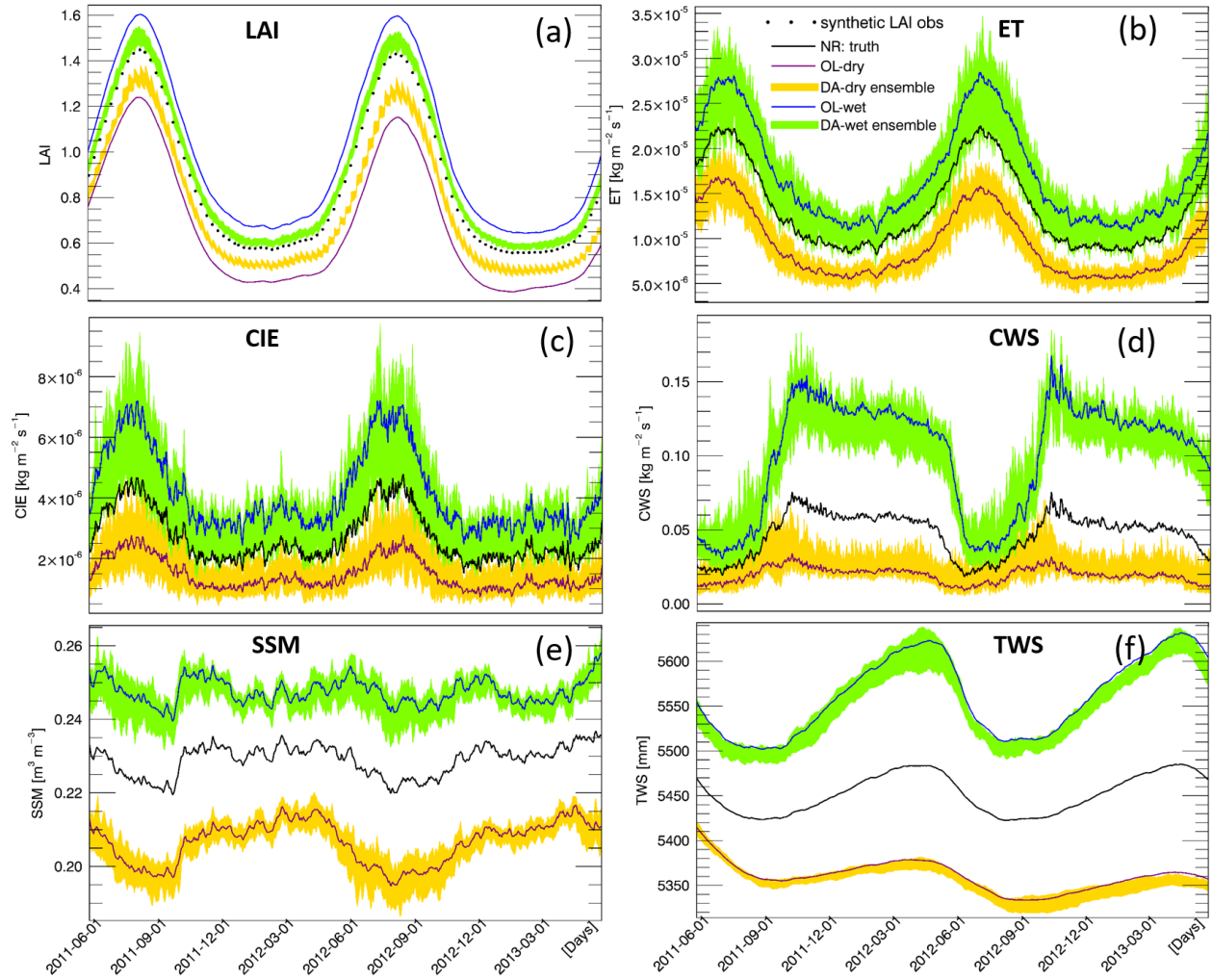
$$223 \quad C = \frac{E_{DA} - E_{OL}}{0 - E_{OL}} \quad \text{Eq. 2}$$

224 where C represents the NIC index and E is the NCRMSE for OL or DA runs. NIC equals to 1
 225 means that DA realizes the maximum possible improvement over the OL; NIC equals to zero
 226 means that DA and OL show the same performance skills; and negative NIC indicates a model
 227 degradation through DA.

228

229 **3. Results and discussion**

230 **3.1. LAI**

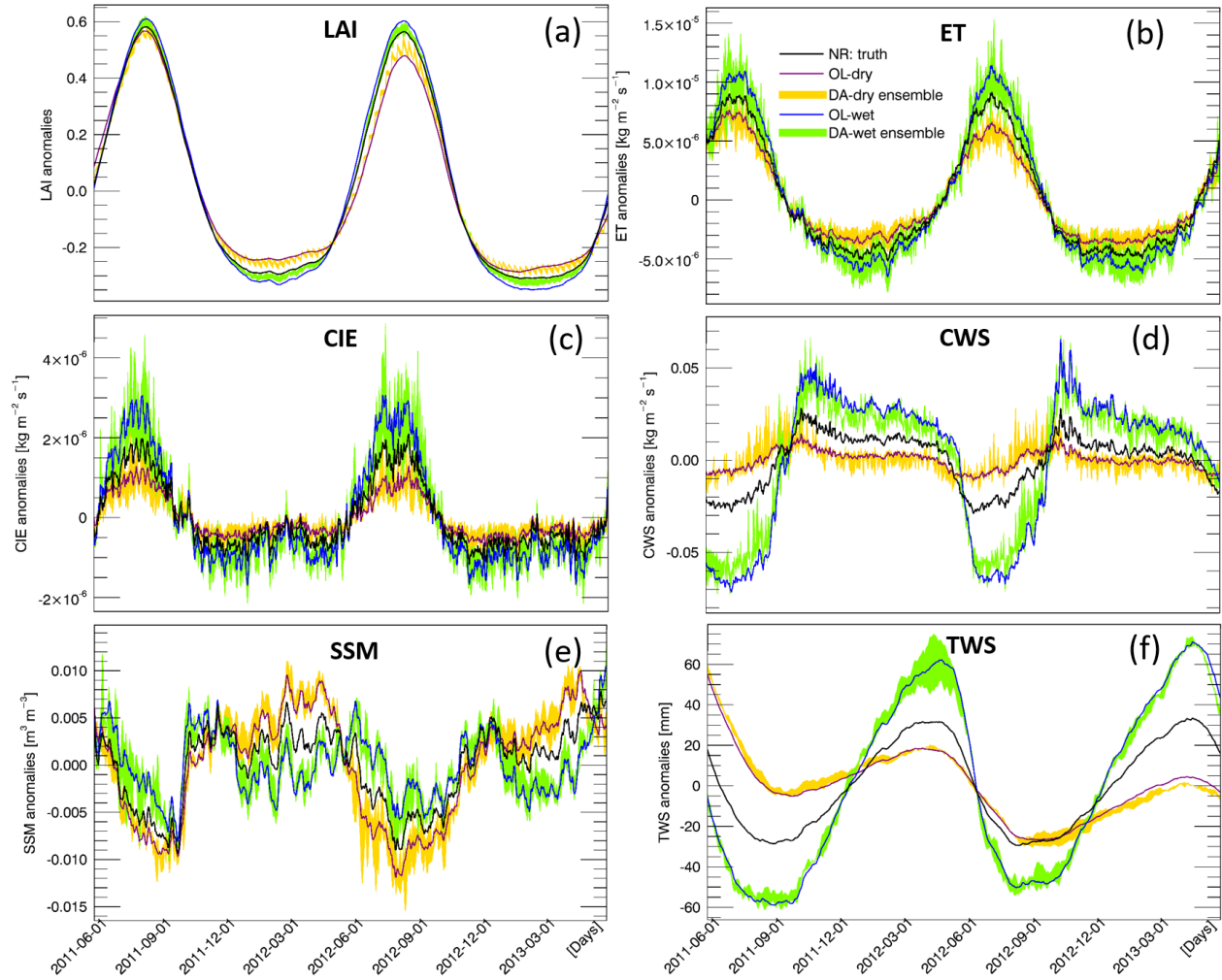


231

232

Figure 3. Global averaged daily values of LAI and five water variables (2011-06-01 to 2013-05-30).

233



234

235

Figure 4. Global averaged daily anomalies of LAI and five water variables (2011-06-01 to 2013-05-30).

236

237 Figure 3a and Figure 4a show time series of global averaged LAI values and corresponding

238 anomalies, respectively. As expected, LAI values are largely impacted by the extreme precipitation

239 conditions. The wet condition introduces more vegetation, while the dry condition limits the

240 vegetation growth throughout the two-year period. The DA procedure effectively corrects the LAI

241 errors caused by the biased precipitation input. The seasonality of LAI anomalies is evident,

242 showing larger variations in DJF and JJA than during the transition periods (MAM and SON). The

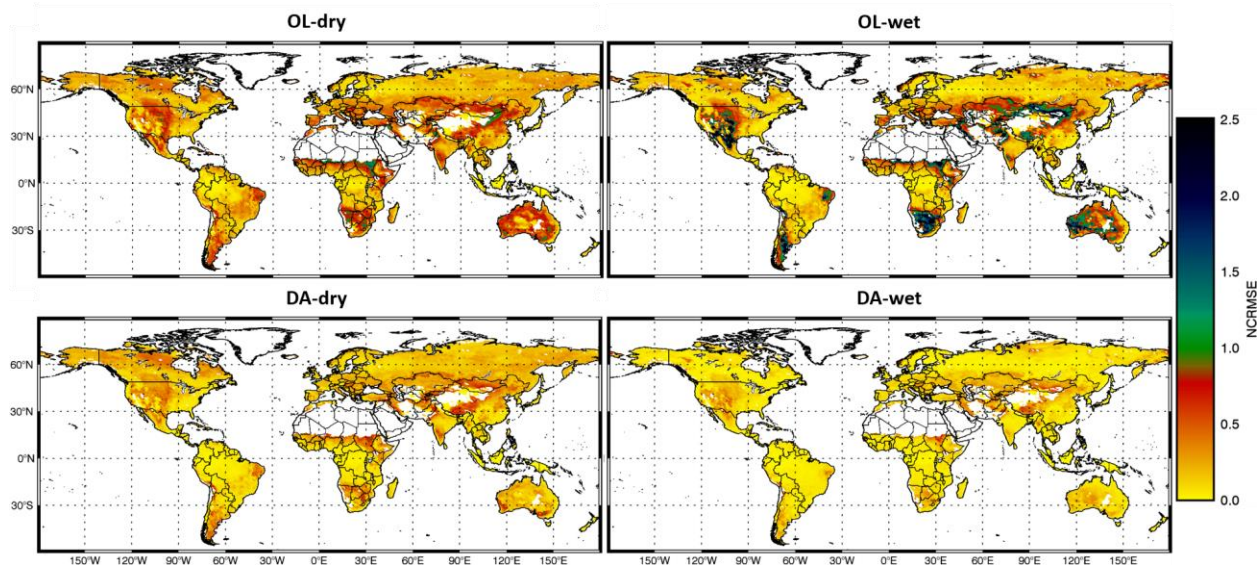
243 OL-wet condition simulation shows larger LAI anomalies than the NR reference, while the OL-

244 dry condition has smaller LAI anomalies than NR. The LAI anomalies obtained from DA runs
245 under both wet and dry conditions are closer to the reference anomalies than the corresponding
246 OL runs. In general, DA performs better in the wet condition experiment than in the dry case.
247 Moreover, the DA runs show lower NCRMSEs than the corresponding OL runs across the globe
248 (Figure 5a), especially over shrublands and grasslands (refer to Figure 1 for land covers).

249 In order to illustrate how LAI assimilation performs for different seasons, Figure 6a and
250 Figure 7a show monthly averages of NCRMSE for LAI across the northern and southern
251 hemispheres, respectively. In the northern hemisphere (Figure 6a), the NCRMSE time series
252 follow clear seasonal patterns. First, the NCRMSE is higher in DJF/MAM and is lower in JJA/SON
253 for both extreme precipitation conditions. The highest NCRMSE values are in March and April,
254 and the lowest values are in July, August, and September. The differences of NCRMSE between
255 OL and the corresponding DA runs tend to be much larger in MAM than in any other seasons,
256 which means that LAI assimilation is more effective in the vegetation growth period. Moreover,
257 the NCRMSE is constantly higher in the dry condition runs than the wet ones, which is due to the
258 fact that the growth of vegetation is sensitive to the lack of water. Differences between wet and
259 dry conditions are much smaller in JJA than in other seasons. In JJA, the vegetation leaves in the
260 north hemisphere are fully developed and the plants can use stomatal closure to preserve water
261 under water limited condition (dry condition). Thus, the NCRMSE of dry condition becomes
262 smaller and does not show much difference from the wet condition. The southern hemisphere
263 (Figure 7a), which does not have a strong climate seasonality, shows more modest seasonal
264 NCRMSE patterns than the northern regions. In general, the NCRMSEs in the southern
265 hemisphere are smaller than the ones in the northern hemisphere all year around. Specifically,

266 NCRMSEs in the southern hemisphere are slightly higher in October, November, and December,
267 when the differences between OL and DA runs are also larger.

268



269

270

Figure 5. Maps of LAI NCRMSE for the OL and DA runs.

271

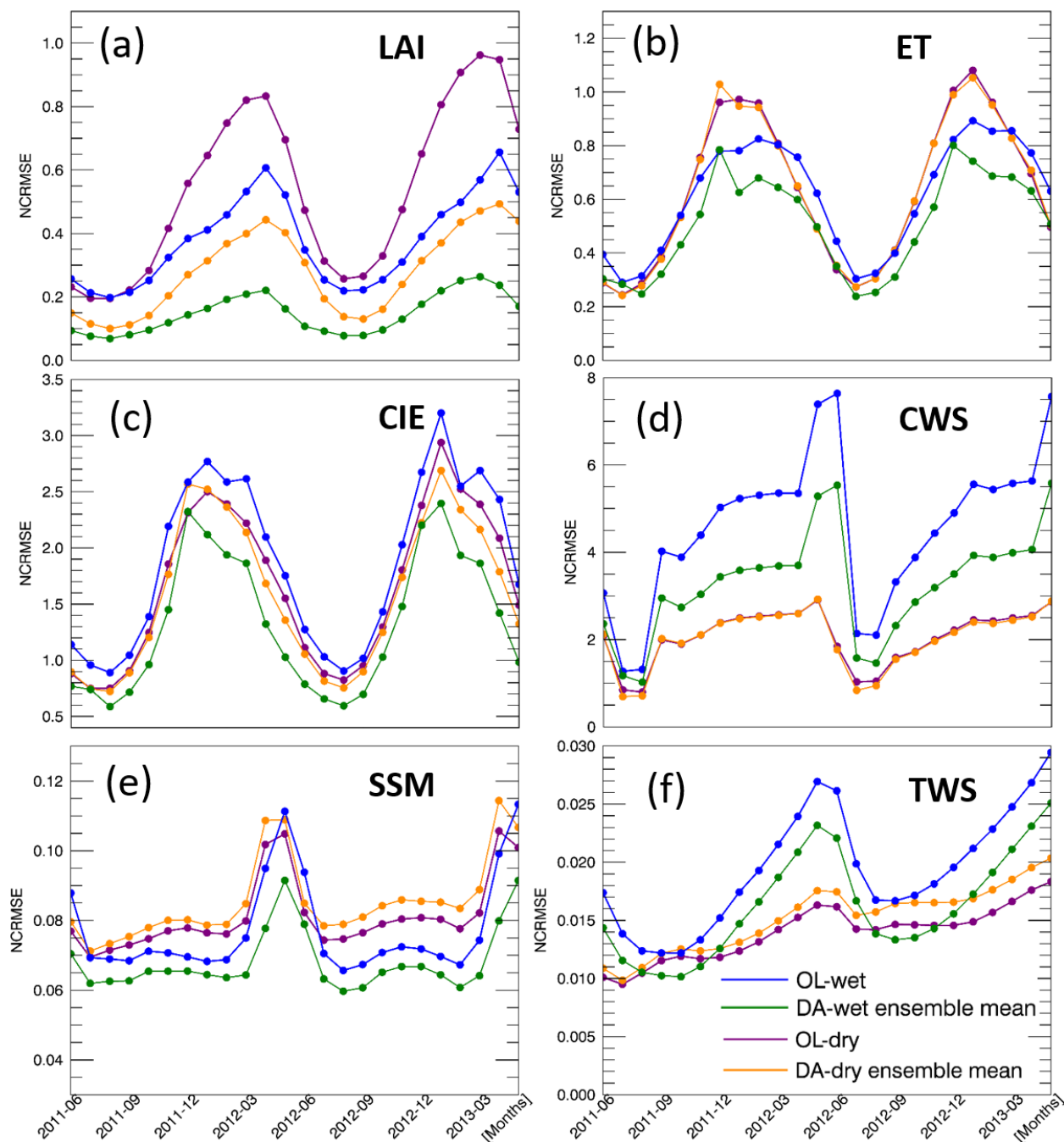
272 3.2. Water fluxes and storages

273 As mentioned in section 2.3, we focus on five water-related variables from the Noah-MP output
274 to evaluate the impact of LAI assimilation on simulating the water cycle (ET, CIE, CWS, SSM,
275 and TWS). Daily time series of global averaged values and corresponding anomalies of the five
276 water variables are shown in Figure 3(b-f) and Figure 4(b-f), respectively. The model well
277 simulates the seasonality of all water fluxes/storages considered here. The OL runs reveal that
278 global average values of all five variables are impacted by the highly biased precipitation
279 conditions. The variations of anomalies for ET, CIE, CWS, and TWS tend to be amplified by the
280 wet condition and tend to be dampened by the dry condition. On the contrary, the anomalies of
281 SSM become larger in dry conditions and become smaller in wet conditions, which is probably

282 due to the limited soil water capacity. The surface soil is more likely to get saturated in wet
283 conditions when the precipitation doubles the original amount, but SSM cannot get larger once the
284 soil is saturated, even if there is more precipitation added to the system. Thus, the range of SSM
285 anomalies in the wet experiment is limited and narrower than in the dry condition. The green and
286 yellow shaded areas represent the ensemble of the DA runs. The anomaly ensembles of the five
287 water variables show slight improvements through DA when precipitation is severely positively
288 biased (wet condition). However, none of these variables shows improvement when the
289 precipitation is severely negatively biased (dry condition) – the anomalies either have no change
290 through the LAI DA (ET, CIE, and CWS) or worsen the OL-dry run (SSM and TWS).

291 To further investigate the efficiency of assimilating LAI in Noah-MP, time series of
292 monthly NCRMSE averages are shown in Figure 6(b-f) and Figure 7(b-f) for all five water
293 variables. The five variables can be divided into two main groups based on their performances:
294 ET/CIE/CWS and SSM/TWS. For the wet bias experiment, DA improves the NCRMSE for all
295 variables. However, LAI assimilation is not able to correct the model when the input precipitation
296 is negatively biased (dry condition). A dry precipitation bias means that the system has
297 (erroneously) less water than in reality (NR in the synthetic experiment). Since no water is
298 otherwise added to the system, LAI DA cannot fully correct water-related model states (such as
299 soil moisture). The NCRMSEs of DA runs are either the same as in the OL runs (ET/CIE/CWS)
300 or worse (SSM/TWS). Specifically, ET/CIE/CWS have larger NCRMSE in the northern
301 hemisphere and much smaller NCRMSEs in the southern hemisphere, but SSM/TWS do not show
302 large differences between north and south. Moreover, ET/CIE/CWS in the northern hemisphere
303 follow a seasonal pattern: NCRMSEs are lower in warm season (JJA) and higher in the colder
304 season (DJF and March). In the southern hemisphere the three variables also have relative higher

305 NCRMSE in the colder season (JJA). On the contrary, SSM/TWS show a different seasonal pattern
 306 that NCRMSEs are larger in the warmer season (April, May, and June) over northern hemisphere.
 307 In southern hemisphere, TWS also has larger NCRMSEs in warmer season (October to April), but
 308 SSM shows higher NCRMSEs in colder season (similar to the ET/CIE/CWS group).



309

310

Figure 6. Monthly averaged NCRMSE for LAI and five water variables over the Northern hemisphere.

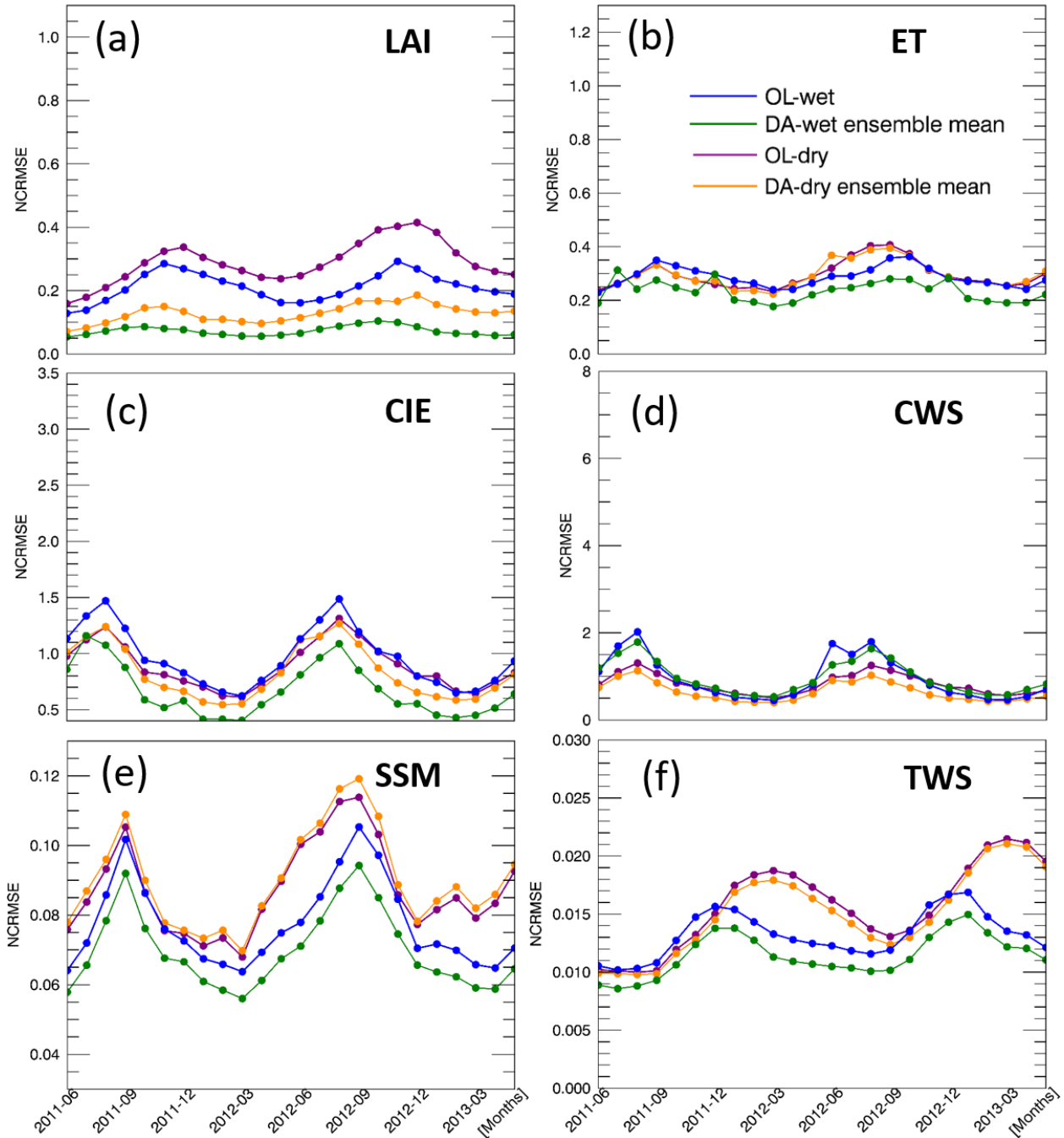


Figure 7. Same as in Figure 6, but for the Southern hemisphere.

311

312

313

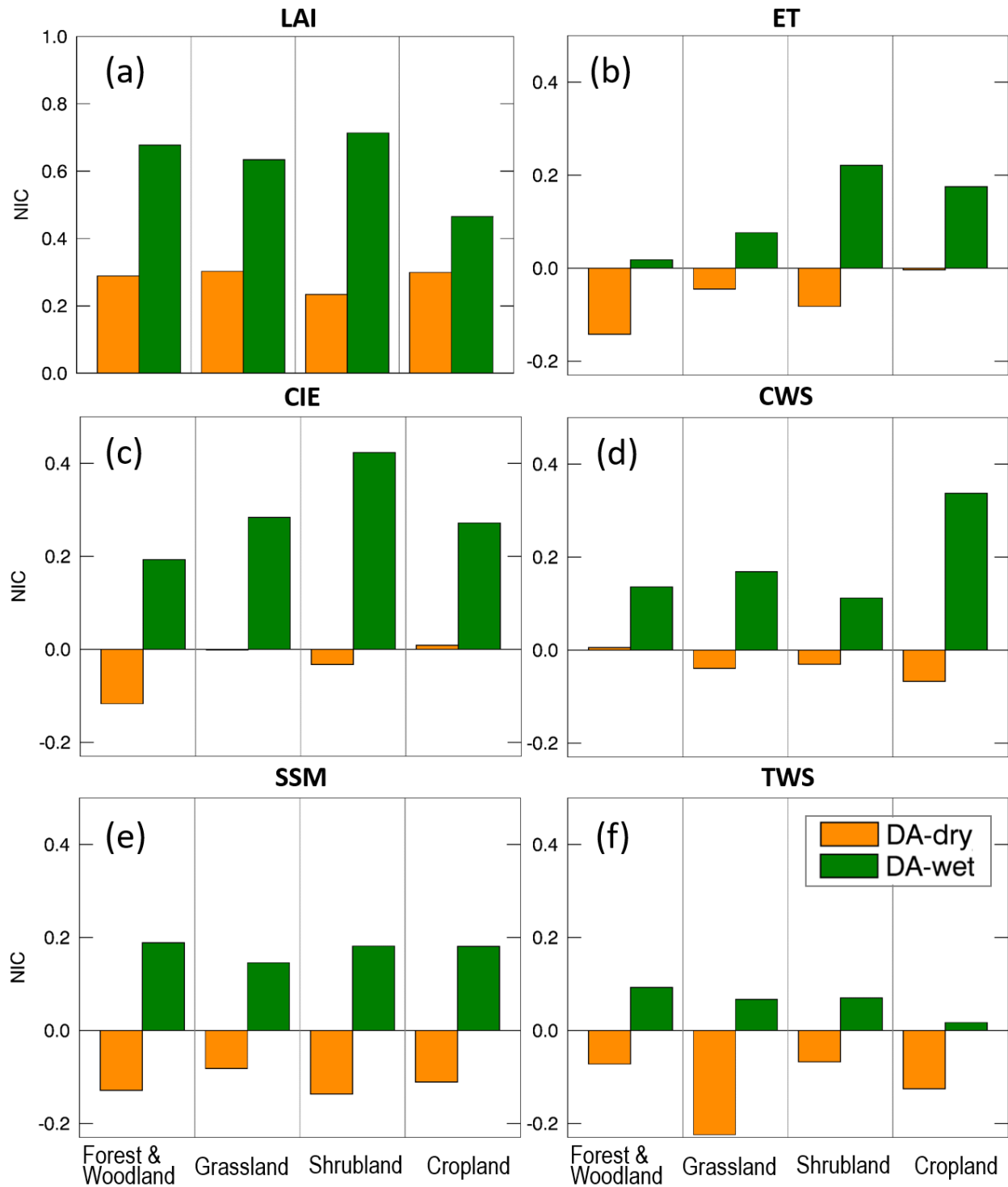
314 The improvements in the model water fluxes and storages through LAI DA are also

315 quantified by the NIC index (defined in Eq. 2). Figure 8 presents comparisons among NIC indices

316 for each water variable analyzed in this study across areas with four different land cover types:

317 forest & woodland, grassland, shrubland, and cropland. In general, LAI DA improves the NIC
318 indices with positively biased input precipitation (DA-wet) but worsens the NIC when negatively
319 biased input precipitation (DA-dry) is considered. Specifically, in wet condition, ET, CIE, and
320 CWS have higher variability over areas with different land cover types, while SSM and TWS have
321 similar NIC values across different land covers. Shrubland and cropland tend to perform better in
322 wet condition except for TWS. In dry condition, the NICs of ET, CIE, and TWS have higher
323 variability than the ones of CWS and SSM. SSM and TWS show very low NIC values in dry
324 condition for almost all land covers. Overall the NIC values of ET, CIE, and CWS are better than
325 the ones of SSM and TWS for all land cover types, though the NICs of ET and CIE over forest &
326 woodland perform very poorly.

327

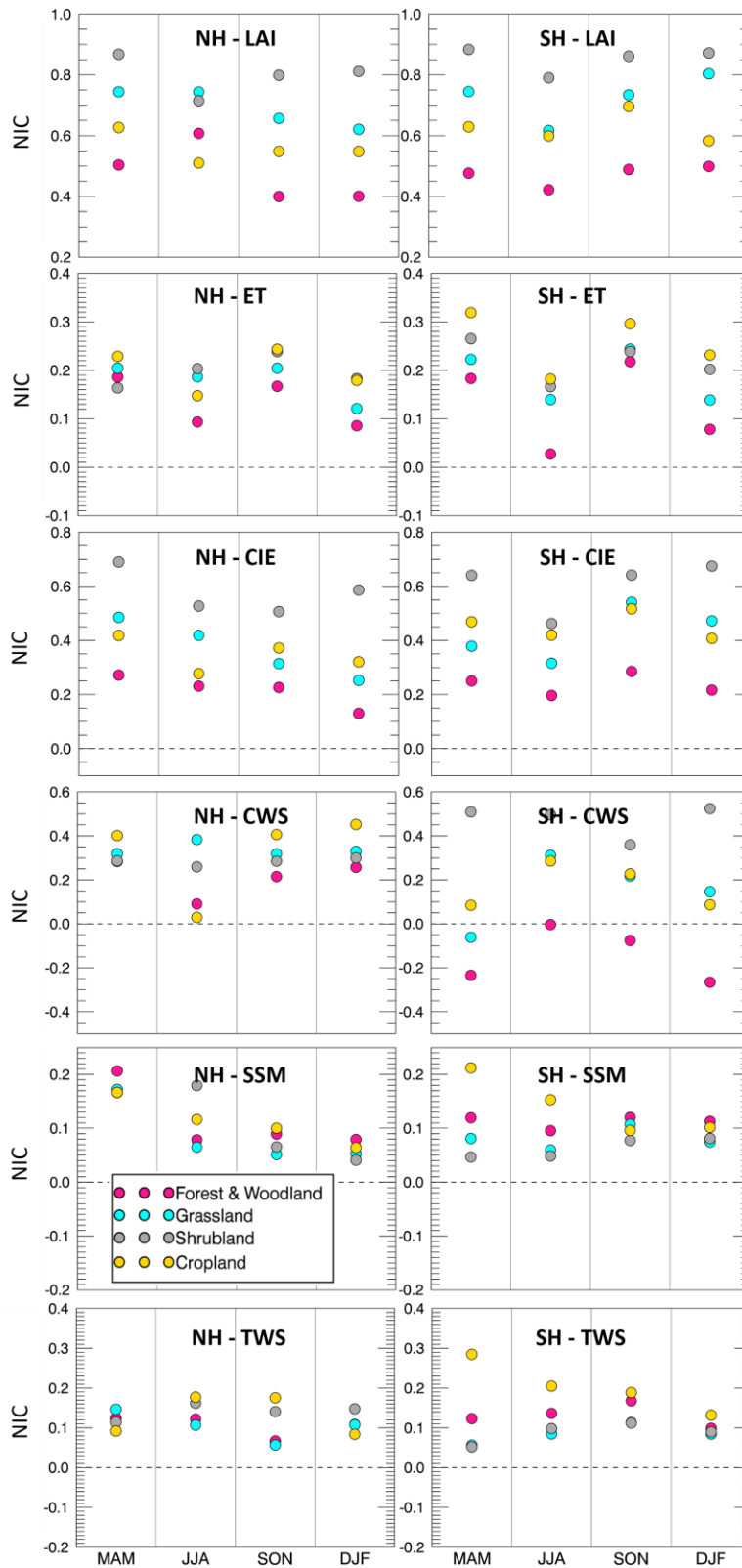


328

329

Figure 8. NIC for different variables and different land cover types for the two DA runs.

330

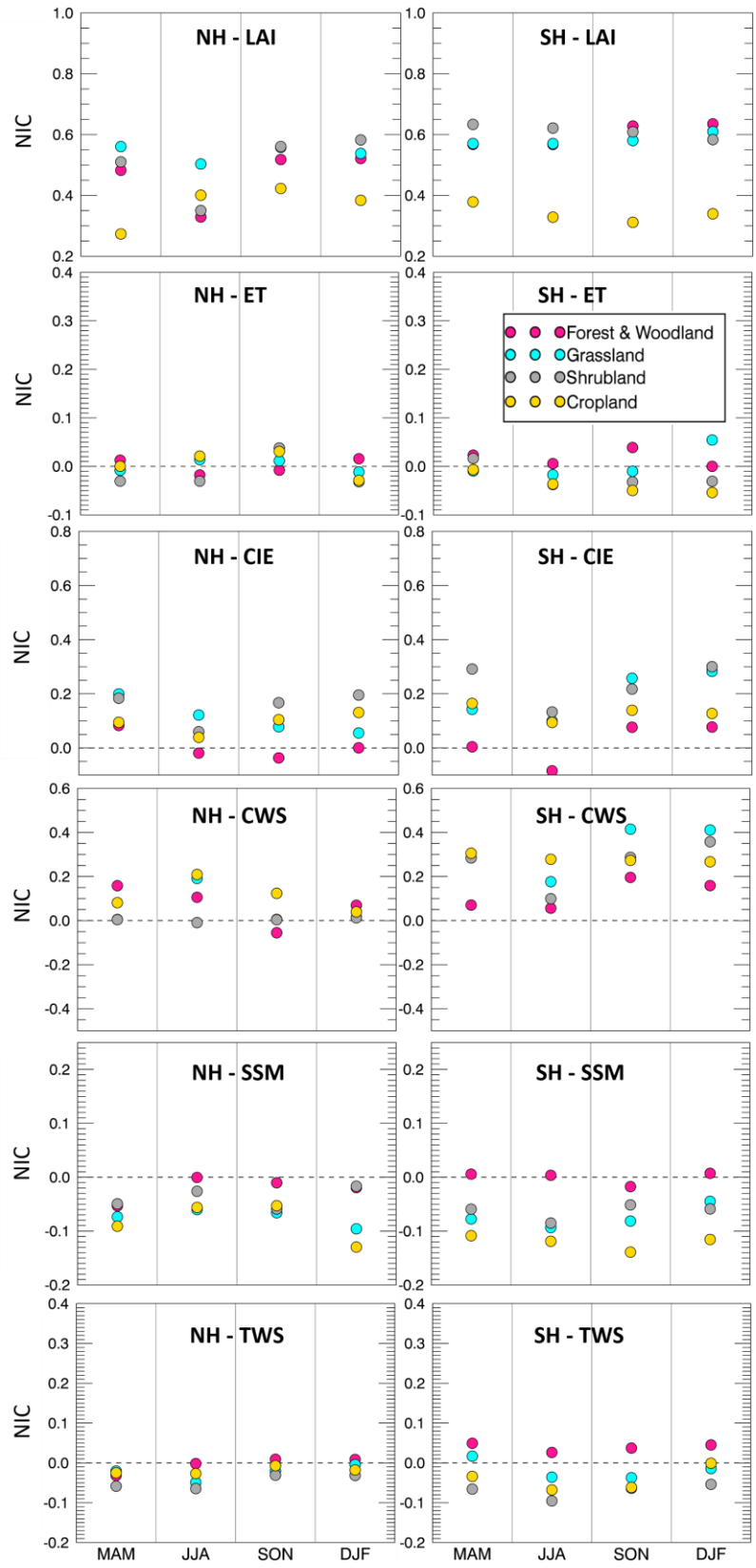


331
332

Figure 9. NIC of five water variables under wet precipitation conditions over northern and southern hemispheres

333

(NH and SH) during different seasons (MAM, JJA, SON, and DJF)



334

335

Figure 10. Same as in Figure 9, but for the dry precipitation experiment.

336

337 The effectiveness of LAI DA therefore varies across the northern and southern hemispheres,
338 different land cover types, as well as different input precipitation biases. To further investigate the
339 influence of LAI assimilation, Figures 8 and 9 present NIC values for each hemisphere, each
340 season, and each of the input precipitation conditions – wet and dry, respectively. For the wet case
341 (Figure 9), NIC is positive in most cases, which means that the five water variables benefit from
342 the LAI assimilation in all seasons and in both hemispheres. The only exception is CWS which
343 has negative NIC values in the southern hemisphere over grassland (in MAM season) and over
344 forest & woodland (in all seasons). In fact, the forest & woodland region tends to have the least
345 improvement through the LAI assimilation among all land cover types. This is probably because
346 forests and woodlands have large water-holding capacity; thus, the change of water amount caused
347 by LAI DA is not enough to improve the water-related variables. In other words, forest and
348 woodland tend to have lower sensitivity in response to the change of precipitation conditions
349 because of their large rooting depth. On the contrary, cropland is very sensitive to precipitation
350 and it benefits the most from the assimilation of LAI for most of the variables. Moreover, NICs of
351 ET/CIE/CWS tend to be smaller than the NICs of SSM and TWS. There is no clear seasonality in
352 the NIC values, though it has a weak tendency to be lower in warm seasons.

353 For the dry condition case (Figure 10), NIC values are much lower than in the wet bias
354 case. Nearly half of the NIC values for the five water-related variables are negative, meaning that
355 DA degrades the OL estimates. Nevertheless, the forest & woodland regions tend to perform better
356 than other land covers in dry condition for SSM and TWS. This is due to large soil reservoir of
357 forests and woodlands, which keeps the model water storage more stable when the input
358 precipitation is affected by large negative biases.

359

360 **3.3. Discussion**

361 Results presented in sections 3.1 and 3.2 indicate that assimilating LAI in Noah-MP improves the
362 model estimates of water fluxes and storages under positively biased precipitation input, but does
363 not benefit most of the selected water variables when the precipitation input is characterized by a
364 negative bias.

365 In the dry condition runs, Noah-MP is fed by only half of the original MERRA-2
366 precipitation used in the NR. Considering that the amount of water in Noah-MP is conservative
367 (since based on a water balance equation), the model has no additional water source in the system,
368 even though the LAI assimilation pushes the model towards more vegetation (that should result in
369 more water). As a matter of fact, introducing more vegetation in the system results in more ET and
370 more root water uptake from the soil, which is most likely the cause for the poor performance of
371 most water fluxes and storages in the DA-dry experiment.

372 On the other hand, the LAI assimilation is found to improve the original OL runs when the
373 input precipitation is positively biased. This is because LAI assimilation is able to help constrain
374 the partitioning of model water storage when there is abundant water in the system, thus, improving
375 the performance of water-related variables. In summary, although the EnKF is run here in a sub-
376 optimal mode (not satisfying the unbiasedness assumption), the assimilation of LAI is shown to
377 have a positive impact on multiple variables and in several regions of the world.

378 Overall the improvement of water variables through LAI assimilation is not remarkable
379 enough to compensate the model degradation caused by the biased precipitation forcing data.
380 Previous studies (Pauwels et al. 2007; Sabater et al. 2007; Barbu et al. 2011; Fairbairn et al. 2017;
381 Albergel et al. 2017) have tested the performance of the joint assimilation of LAI and soil moisture

382 over regional domains and showed promising results. However, no experiment was performed at
383 the global scale. Future work could investigate a multi-variate data assimilation system that
384 concurrently merges both LAI and soil moisture (or TWS) observations globally.

385

386 **4. Conclusions**

387 This study evaluates the efficiency of assimilating vegetation information (i.e., LAI synthetic
388 observations) within a land surface model (Noah-MP 3.6) when the precipitation forcing data are
389 strongly biased (either positively or negatively). Two OSSEs that use an EnKF algorithm for LAI
390 assimilation are performed at global scale during June 2011 – May 2013. The experiments use
391 MERRA-2 as meteorological forcing data. The OL and DA runs are evaluated against a synthetic
392 “truth” from a nature run, in which the MERRA-2 precipitation is neither perturbed nor biased.
393 The performance of the proposed framework is evaluated for several model output, including LAI
394 estimates and five water-related variables (ET, CIE, CWS, SSM, and TWS).

395 Overall the EnKF LAI assimilation procedure effectively reduces the LAI error under
396 positively (wet case) and the negatively (dry case) biased precipitation conditions. For the five
397 selected water flux or storage variables, LAI DA improves the model estimates when the model
398 input precipitation is positively biased, but tends to worsen the OL estimates for some of those
399 variables when the input precipitation is negatively biased. Specifically, SSM and TWS estimates
400 are degraded in the DA-dry run with respect to the OL-dry run, while ET, CIE, and CWS do not
401 present large changes when LAI is assimilated in the dry bias run. The poor performance of LAI
402 DA under dry condition is mainly attributed to the fact that the amount of water in Noah-MP is
403 conservative. The LAI assimilation in dry condition introduces more vegetation, which requires

404 more water in the system to replenish the soil water supply. However, the model has no additional
405 source of water, since the input precipitation is negatively biased.

406 Although a blind bias case (e.g., unknown biases in the precipitation forcing dataset) is
407 presented here in which the EnKF is run in a sub-optimal mode, the assimilation of LAI
408 observations is proven useful to improve several model output variables. Future research should
409 focus on alternative DA methods, such as updating other related model states while assimilating
410 LAI observations, perturbing the model initial condition and model parameters, and/or assimilating
411 actual satellite-based LAI observations (e.g., MODIS, GLASS) at the global scale to verify the
412 efficiency of the proposed vegetation DA framework. This may be particularly useful in
413 agricultural areas, where the vegetation conditions are largely impacted by cropping schedules
414 (Kumar et al. 2019b). Moreover, future work could investigate multi-variate DA techniques that
415 combine the assimilation of several variables (such as LAI, soil moisture, and TWS) at the global
416 scale.

417

418

419

420 ***Acknowledgements:*** This research is sponsored by the NASA Modeling, Analysis, and
421 Prediction (MAP) Program (80NSSC17K0109). We would also like to acknowledge the
422 computational resources and support from the ARGO HPC Cluster team at George Mason
423 University.

424 **References**

- 425 Adegoke, J. O. and Carleton, A. M.: Relations between soil moisture and satellite vegetation
426 indices in the US Corn Belt, *J. Hydrometeorol.*, 3, 395-405, [https://doi.org/10.1175/1525-7541\(2002\)003<0395:RBSMAS>2.0.CO;2](https://doi.org/10.1175/1525-7541(2002)003<0395:RBSMAS>2.0.CO;2), 2002.
- 428 Albergel, C., Munier, S., Leroux, D.J., Dewaele, H., Fairbairn, D., Barbu, A.L., Gelati, E., Dorigo,
429 W., Faroux, S., Meurey, C. and Le Moigne, P.: Sequential assimilation of satellite-derived
430 vegetation and soil moisture products using SURFEX_v8. 0: LDAS-Monde assessment over
431 the Euro-Mediterranean area, *Geosci. Model Dev.*, 10, 3889-3912,
432 <https://doi.org/10.5194/gmd-10-3889-2017>, 2017. Andreadis, K. M. and Lettenmaier, D. P.:
433 Assimilating remotely sensed snow observations into a macroscale hydrology model, *Adv.*
434 *Water Resour.*, 29, 872-886, <https://doi.org/10.1016/j.advwatres.2005.08.004>, 2006.
- 435 Arora, V.: Modeling vegetation as a dynamic component in soil - vegetation - atmosphere transfer
436 schemes and hydrological models, *Rev. Geophys.*, 40, 3-1,
437 <https://doi.org/10.1029/2001RG000103>, 2002.
- 438 Ball, J. T., Woodrow, I. E. and Berry, J. A.: A model predicting stomatal conductance and its
439 contribution to the control of photosynthesis under different environmental conditions, in:
440 *Progress in photosynthesis research*, Springer, Dordrecht, 221-224,
441 https://doi.org/10.1007/978-94-017-0519-6_48, 1987.
- 442 Barbu, A. L., Calvet, J. C., Mahfouf, J. F., Albergel, C., and Lafont, S.: Assimilation of Soil
443 Wetness Index and Leaf Area Index into the ISBA-A-gs land surface model: grassland case
444 study, *Biogeosciences*, 8, 1971-1986, <https://doi.org/10.5194/bg-8-1971-2011>, 2011.
- 445 Baret, F., Hagolle, O., Geiger, B., Bicheron, P., Miras, B., Huc, M., Berthelot, B., Niño, F., Weiss,
446 M., Samain, O. and Roujean, J. L.: LAI, fAPAR and fCover CYCLOPES global products
447 derived from VEGETATION: Part 1: Principles of the algorithm, *Remote Sens. Environ.*, 110,
448 275-286, <https://doi.org/10.1016/j.rse.2007.02.018>, 2007.
- 449 Cohen, W. B. and Justice, C. O.: Validating MODIS terrestrial ecology products: linking in situ
450 and satellite measurements, *Remote Sens. Environ.*, 70, 1-3, 1999.
- 451 Cracknell, A. P.: *Advanced very high resolution radiometer AVHRR*, CRC Press, 543, 1997.
- 452 Crow, W. T. and Wood, E. F.: The assimilation of remotely sensed soil brightness temperature
453 imagery into a land surface model using ensemble Kalman filtering: A case study based on
454 ESTAR measurements during SGP97, *Adv. Water Resour.*, 26, 137-149,
455 [https://doi.org/10.1016/S0309-1708\(02\)00088-X](https://doi.org/10.1016/S0309-1708(02)00088-X), 2003.
- 456 De Lannoy, G.J., Reichle, R.H., Arsenault, K.R., Houser, P.R., Kumar, S., Verhoest, N.E. and
457 Pauwels, V.R.: Multiscale assimilation of Advanced Microwave Scanning Radiometer–EOS
458 snow water equivalent and Moderate Resolution Imaging Spectroradiometer snow cover
459 fraction observations in northern Colorado, *Water Resour. Res.*, 48,
460 <https://doi.org/10.1029/2011WR010588>, 2012
- 461 Di, L., Rundquist, D. C. and Han, L.: Modelling relationships between NDVI and precipitation
462 during vegetative growth cycles, *Int. J. Remote Sens.*, 15, 2121-2136,
463 <https://doi.org/10.1080/01431169408954231>, 1994.

464 Dickinson, R. E., Shaikh, M., Bryant, R. and Graumlich, L.: Interactive canopies for a climate
465 model, *J. Climate*, 11(, 2823-2836, <https://doi.org/10.1175/1520->
466 0442(1998)011<2823:ICFACM>2.0.CO;2, 1998.

467 Druel, A., Ciais, P., Krinner, G., and Peylin, P.: Modeling the vegetation dynamics of northern
468 shrubs and mosses in the ORCHIDEE land surface model, *J. Adv. Model Earth Sy.*, 11, 2020-
469 2035, <https://doi.org/10.1029/2018MS001531>, 2019.

470 Durand, M. and Margulis, S. A.: Effects of uncertainty magnitude and accuracy on assimilation of
471 multiscale measurements for snowpack characterization, *J. Geophys. Res.: Atmos.*, 113,
472 D02105, <https://doi.org/10.1029/2007JD008662>, 2008.

473 Evensen, G.: The ensemble Kalman filter: Theoretical formulation and practical implementation,
474 *Ocean dynam.*, 53, 343-367, <https://doi.org/10.1007/s10236-003-0036-9>, 2003.

475 Fairbairn, D., Barbu, A., Napoly, A., Albergel, C., Mahfouf, J. F., and Calvet, J. C.: The effect of
476 satellite-derived surface soil moisture and leaf area index land data assimilation on streamflow
477 simulations over France. *HESS*, 21, 2015-2033, <https://doi.org/10.5194/hess-21-2015-2017>,
478 2017

479 Farrar, T. J., Nicholson, S. E. and Lare, A. R.: The influence of soil type on the relationships
480 between NDVI, rainfall, and soil moisture in semiarid Botswana. II. NDVI response to soil
481 moisture, *Remote Sens. Environ.*, 50, 121-133, [https://doi.org/10.1016/0034-4257\(94\)90039-](https://doi.org/10.1016/0034-4257(94)90039-6)
482 6, 1994.

483 Fisher, R. A., Koven, C. D., Anderegg, W. R., Christoffersen, B. O., Dietze, M. C., Farrior, C. E.,
484 Holm, J. A., Hurtt, G. C., Knox, R. G., Lawrence, P. J. and Lichstein, J. W.: Vegetation
485 demographics in Earth System Models: A review of progress and priorities, *Global Change*
486 *Biol.*, 24, 35-54, <https://doi.org/10.1111/gcb.13910>, 2018.

487 Foley, J. A., Prentice, I. C., Ramankutty, N., Levis, S., Pollard, D., Sitch, S. and Haxeltine, A.: An
488 integrated biosphere model of land surface processes, terrestrial carbon balance, and
489 vegetation dynamics, *Global Biogeochem. Cy.*, 10, 603-628,
490 <https://doi.org/10.1029/96GB02692>, 1996.

491 Gelaro, R., McCarty, W., Suárez, M. J., Todling, R., Molod, A., Takacs, L., Randles, C. A.,
492 Darmenov, A., Bosilovich, M. G., Reichle, R. and Wargan, K.: The modern-era retrospective
493 analysis for research and applications, version 2 (MERRA-2), *J. Climate*, 30, 5419-5454,
494 <https://doi.org/10.1175/JCLI-D-16-0758.1>, 2017.

495 Ghatak, D., Zaitchik, B., Kumar, S., Matin, M., Bajracharya, B., Hain, C. and Anderson, M.:
496 Influence of Precipitation Forcing Uncertainty on Hydrological Simulations with the NASA
497 South Asia Land Data Assimilation System, *Hydrology*, 5, 57,
498 <https://doi.org/10.3390/hydrology5040057>, 2018.

499 Gibelin, A. L., Calvet, J. C., Roujean, J. L., Jarlan, L. and Los, S. O.: Ability of the land surface
500 model ISBA - A - gs to simulate leaf area index at the global scale: Comparison with
501 satellites products, *J. Geophys. Res.: Atmos.*, 111, D18102,
502 <https://doi.org/10.1029/2005JD006691>, 2006.

503 Hansen, M. C., DeFries, R. S., Townshend, J. R. and Sohlberg, R.: Global land cover classification
504 at 1 km spatial resolution using a classification tree approach, *Int. J. Remote Sens.*, 21, 1331-
505 1364, <https://doi.org/10.1080/014311600210209>, 2000.

506 Justice, C. O., Townshend, J. R. G., Vermote, E. F., Masuoka, E., Wolfe, R. E., Saleous, N., Roy,
507 D. P. and Morisette, J. T.: An overview of MODIS Land data processing and product status,
508 Remote Sens. Environ., 83, 3-15, [https://doi.org/10.1016/S0034-4257\(02\)00084-6](https://doi.org/10.1016/S0034-4257(02)00084-6), 2002.

509 Kim, Y. and Wang, G.: Impact of vegetation feedback on the response of precipitation to
510 antecedent soil moisture anomalies over North America J. Hydrometeorol., 8, 534-550,
511 <https://doi.org/10.1175/JHM612.1>, 2007.

512 Krinner, G., Viovy, N., de Noblet - Ducoudré, N., Ogée, J., Polcher, J., Friedlingstein, P., Ciais,
513 P., Sitch, S. and Prentice, I. C.: A dynamic global vegetation model for studies of the coupled
514 atmosphere - biosphere system, Global Biogeochem. Cy., 19, GB1015,
515 <https://doi.org/10.1029/2003GB002199>, 2005.

516 Kucharik, C. J., Foley, J. A., Delire, C., Fisher, V. A., Coe, M. T., Lenters, J. D., Young - Molling,
517 C., Ramankutty, N., Norman, J. M. and Gower, S. T.: Testing the performance of a dynamic
518 global ecosystem model: water balance, carbon balance, and vegetation structure, Global
519 Biogeochem. Cy., 14, 795-825, <https://doi.org/10.1029/1999GB001138>, 2000.

520 Kumar, S. V., Peters-Lidard, C. D., Tian, Y., Houser, P. R., Geiger, J., Olden, S., Lighty, L.,
521 Eastman, J. L., Doty, B., Dirmeyer, P. and Adams, J.: Land information system: An
522 interoperable framework for high resolution land surface modeling, Environ. Modell. Softw.,
523 21, 1402-1415, <https://doi.org/10.1016/j.envsoft.2005.07.004>, 2006.

524 Kumar, S. V., Peters-Lidard, C., Tian, Y., Reichle, R., Geiger, J., Alonge, C., Eylander, J. and
525 Houser, P.: An integrated hydrologic modeling and data assimilation framework, Computer,
526 41, 52-59, <https://doi.org/10.1109/MC.2008.475>, 2008.

527 Kumar, S. V., Peters-Lidard, C. D., Mocko, D., Reichle, R., Liu, Y., Arsenault, K. R., Xia, Y., Ek,
528 M., Riggs, G., Livneh, B. and Cosh, M.: Assimilation of remotely sensed soil moisture and
529 snow depth retrievals for drought estimation, J. Hydrometeorol., 15, 2446-2469,
530 <https://doi.org/10.1175/JHM-D-13-0132.1>, 2014.

531 Kumar, S.V., Zaitchik, B.F., Peters-Lidard, C.D., Rodell, M., Reichle, R., Li, B., Jasinski, M.,
532 Mocko, D., Getirana, A., De Lannoy, G. and Cosh, M.H.: Assimilation of gridded GRACE
533 terrestrial water storage estimates in the North American Land Data Assimilation System, J.
534 Hydrometeorol., 17, 1951-1972, <https://doi.org/10.1175/JHM-D-15-0157.1>, 2016

535 Kumar, S. V., Jasinski, M., Mocko, D. M., Rodell, M., Borak, J., Li, B., Beaudoin, H. K. and
536 Peters-Lidard, C. D.: NCA-LDAS land analysis: Development and performance of a
537 multisensor, multivariate land data assimilation system for the National Climate Assessment,
538 J. Hydrometeorol., 20, 1571-1593, <https://doi.org/10.1175/JHM-D-17-0125.1>, 2019.

539 Kumar, S. V., Mocko, D. M., Wang, S., Peters-Lidard, C. D. and Borak, J.: Assimilation of
540 remotely sensed Leaf Area Index into the Noah-MP land surface model: Impacts on water and
541 carbon fluxes and states over the Continental US, J. Hydrometeorol., 20, 1359-1377,
542 <https://doi.org/10.1175/JHM-D-18-0237.1>, 2019.

543 Ling, X. L., Fu, C. B., Guo, W. D. and Yang, Z. L.: Assimilation of remotely sensed LAI into
544 CLM4CN using DART, J. Adv. Model. Earth Sy., <https://doi.org/10.1029/2019MS001634>,
545 2019.

546 Liu, Y., Liu, R. and Chen, J. M.: Retrospective retrieval of long - term consistent global leaf area
547 index (1981 - 2011) from combined AVHRR and MODIS data, *J. Geophys. Res.: Biogeo.*,
548 117, G04003, <https://doi.org/10.1029/2012JG002084>, 2012.

549 Liu, Y., Peters - Lidard, C.D., Kumar, S.V., Arsenault, K.R. and Mocko, D.M.: Blending
550 satellite - based snow depth products with in situ observations for streamflow predictions in
551 the Upper Colorado River Basin, *Water Resour. Res.*, 51, 1182-1202,
552 <https://doi.org/10.1002/2014WR016606>, 2015

553 Morisette, J. T., Privette, J. L. and Justice, C. O.: A framework for the validation of MODIS land
554 products, *Remote Sens. Environ.*, 83, 77-96, [https://doi.org/10.1016/S0034-4257\(02\)00088-](https://doi.org/10.1016/S0034-4257(02)00088-3)
555 3, 2002.

556 Myneni, R. B., Hoffman, S., Knyazikhin, Y., Privette, J. L., Glassy, J., Tian, Y., Wang, Y., Song,
557 X., Zhang, Y., Smith, G. R. and Lotsch, A.: Global products of vegetation leaf area and
558 fraction absorbed PAR from year one of MODIS data, *Remote Sens. Environ.*, 83, 214-231,
559 [https://doi.org/10.1016/S0034-4257\(02\)00074-3](https://doi.org/10.1016/S0034-4257(02)00074-3), 2002.

560 Niu, G. Y. and Yang, Z. L.: An observation - based formulation of snow cover fraction and its
561 evaluation over large North American river basins, *J. Geophys. Res.: Atmos.*, 112, D21101,
562 <https://doi.org/10.1029/2007JD008674>, 2007.

563 Niu, G. Y., Yang, Z. L., Mitchell, K. E., Chen, F., Ek, M. B., Barlage, M., Kumar, A., Manning,
564 K., Niyogi, D., Rosero, E. and Tewari, M.: The community Noah land surface model with
565 multiparameterization options (Noah - MP): 1. Model description and evaluation with local -
566 scale measurements, *J. Geophys. Res.: Atmos.*, 116, D12109,
567 <https://doi.org/10.1029/2010JD015139>, 2011.

568 Pagano, T. S. and Durham, R. M.: Moderate resolution imaging spectroradiometer (MODIS), in:
569 Proceedings of SPIE 1939 Sensor Systems for the Early Earth Observing System Platforms,
570 International Society for Optics and Photonics, Orlando, FL, United States, 25 August 1993,
571 2-17, <https://doi.org/10.1117/12.152835>, 1993

572 Pan, M. and Wood, E. F.: Data assimilation for estimating the terrestrial water budget using a
573 constrained ensemble Kalman filter, *J. Hydrometeorol.*, 7, 534-547,
574 <https://doi.org/10.1175/JHM495.1>, 2006.

575 Pauwels, V. R. and De Lannoy, G. J.: Improvement of modeled soil wetness conditions and
576 turbulent fluxes through the assimilation of observed discharge, *J. Hydrometeorol.*, 7, 458-
577 477, <https://doi.org/10.1175/JHM490.1>, 2006.

578 Pauwels, V. R., Verhoest, N. E., De Lannoy, G. J., Guissard, V., Lucau, C. and Defourny, P.:
579 Optimization of a coupled hydrology-crop growth model through the assimilation of observed
580 soil moisture and leaf area index values using an ensemble Kalman filter, *Water Resour. Res.*,
581 43, W04421, <https://doi.org/10.1029/2006WR004942>, 2007.

582 Peters-Lidard, C. D., Houser, P. R., Tian, Y., Kumar, S. V., Geiger, J., Olden, S., Lighty, L., Doty,
583 B., Dirmeyer, P., Adams, J. and Mitchell, K. High-performance Earth system modeling with
584 NASA/GSFC's Land Information System, *Innovations Syst. Softw. Eng.*, 3, 157-165,
585 <https://doi.org/10.1007/s11334-007-0028-x>, 2007.

586 Privette, J. L., Myneni, R. B., Knyazikhin, Y., Mukelabai, M., Roberts, G., Tian, Y., Wang, Y. and
587 Leblanc, S. G.: Early spatial and temporal validation of MODIS LAI product in the Southern
588 Africa Kalahari, *Remote Sens. Environ.*, 83, 232-243, [https://doi.org/10.1016/S0034-](https://doi.org/10.1016/S0034-4257(02)00075-5)
589 [4257\(02\)00075-5](https://doi.org/10.1016/S0034-4257(02)00075-5), 2002.

590 Reichle, R. H., McLaughlin, D. B. and Entekhabi, D.: Hydrologic data assimilation with the
591 ensemble Kalman filter, *Mon. Weather Rev.*, 130, 103-114, [https://doi.org/10.1175/1520-](https://doi.org/10.1175/1520-0493(2002)130<0103:HDAWTE>2.0.CO;2)
592 [0493\(2002\)130<0103:HDAWTE>2.0.CO;2](https://doi.org/10.1175/1520-0493(2002)130<0103:HDAWTE>2.0.CO;2), 2002.

593 Reichle, R. H., Walker, J. P., Koster, R. D. and Houser, P. R.: Extended versus ensemble Kalman
594 filtering for land data assimilation, *J. Hydrometeorol.*, 3, 728-740,
595 [https://doi.org/10.1175/1525-7541\(2002\)003<0728:EVEKFF>2.0.CO;2](https://doi.org/10.1175/1525-7541(2002)003<0728:EVEKFF>2.0.CO;2), 2002.

596 Reichle, R. H., Koster, R. D., Liu, P., Mahanama, S. P., Njoku, E. G. and Owe, M.: Comparison
597 and assimilation of global soil moisture retrievals from the Advanced Microwave Scanning
598 Radiometer for the Earth Observing System (AMSR - E) and the Scanning Multichannel
599 Microwave Radiometer (SMMR), *J. Geophys. Res.: Atmos.*, 112, D09108,
600 <https://doi.org/10.1029/2006JD008033>, 2007.

601 Reichle, R. H., Kumar, S. V., Mahanama, S. P., Koster, R. D. and Liu, Q.: Assimilation of satellite-
602 derived skin temperature observations into land surface models, *J. Hydrometeorol.*, 11, 1103-
603 1122, <https://doi.org/10.1175/2010JHM1262.1>, 2010.

604 Richard, Y. and Pocard, I.: A statistical study of NDVI sensitivity to seasonal and interannual
605 rainfall variations in Southern Africa, *Int. J. Remote Sens.*, 19, 2907-2920,
606 <https://doi.org/10.1080/014311698214343>, 1998.

607 Sabater, J. M., Rüdiger, C., Calvet, J. C., Fritz, N., Jarlan, L. and Kerr, Y.: Joint assimilation of
608 surface soil moisture and LAI observations into a land surface model, *Agr. Forest Meteorol.*,
609 148, 1362-1373, <https://doi.org/10.1016/j.agrformet.2008.04.003>, 2008.

610 Tian, Y., Woodcock, C. E., Wang, Y., Privette, J. L., Shabanov, N. V., Zhou, L., Zhang, Y.,
611 Buermann, W., Dong, J., Veikkanen, B. and Häme, T.: Multiscale analysis and validation of
612 the MODIS LAI product: I. Uncertainty assessment, *Remote Sens. Environ.*, 83, 414-430,
613 [https://doi.org/10.1016/S0034-4257\(02\)00047-0](https://doi.org/10.1016/S0034-4257(02)00047-0), 2002.

614 Wang, G. and Eltahir, E. A.: Role of vegetation dynamics in enhancing the low - frequency
615 variability of the Sahel rainfall, *Water Resour. Res.*, 36, 1013-1021,
616 <https://doi.org/10.1029/1999WR900361>, 2000.

617 Wang, G., Sun, S. and Mei, R.: Vegetation dynamics contributes to the multi - decadal variability
618 of precipitation in the Amazon region, *Geophys. Res. Lett.*, 38, L19703,
619 <https://doi.org/10.1029/2011GL049017>, 2011.

620 Woodward, F. I. and Lomas, M. R.: Vegetation dynamics—simulating responses to climatic change,
621 *Biol. Rev.*, 79, 643-670, <https://doi.org/10.1017/S1464793103006419>, 2004.

622 Xiao, Z., Liang, S., Wang, J., Chen, P., Yin, X., Zhang, L. and Song, J. Use of general regression
623 neural networks for generating the GLASS leaf area index product from time-series MODIS
624 surface reflectance, *IEEE T. Geosci. Remote*, 52, 209-223,
625 <https://doi.org/10.1109/TGRS.2013.2237780>, 2013.

- 626 Yang, Z. L., Niu, G. Y., Mitchell, K. E., Chen, F., Ek, M. B., Barlage, M., Longuevergne, L.,
627 Manning, K., Niyogi, D., Tewari, M. and Xia, Y.: The community Noah land surface model
628 with multiparameterization options (Noah - MP): 2. Evaluation over global river basins, J.
629 Geophys. Res.: Atmos., 116, D12110, <https://doi.org/10.1029/2010JD015140>, 2011.
- 630 Yoon, Y., Kumar, S.V., Forman, B.A., Zaitchik, B.F., Kwon, Y., Qian, Y., Rupper, S., Maggioni,
631 V., Houser, P., Kirschbaum, D. and Richey, A.: Evaluating the uncertainty of terrestrial water
632 budget components over High Mountain Asia, Front. Earth Sci., 7,
633 <https://doi.org/10.3389/feart.2019.00120>, 2019
- 634 Zhou, Y., McLaughlin, D. and Entekhabi, D.: Assessing the performance of the ensemble Kalman
635 filter for land surface data assimilation, Mon. Weather Rev., 134, 2128-2142,
636 <https://doi.org/10.1175/MWR3153.1>, 2006.